Interaction of a Short Antimicrobial Peptide on Charged Lipid Bilayer: A Case Study on Aurein 1.2 Peptide

Shuo Qian [1, 2], Piotr A. Zolnierczuk[1]*

Author Affiliation

1. Neutron Scattering Division, Oak Ridge National Laboratory, Oak Ridge, TN 37830
2. Second Target Station, Oak Ridge National Laboratory, Oak Ridge, TN 37830

Corresponding Authors

*Shuo Qian: qians@ornl.gov, +1-865-241-1934

ABSTRACT

Aurein 1.2 is a short but potent α-helical membrane-active antimicrobial peptide that has shown inhibition on a broad spectrum of bacteria and anti-cancer cell activity. With well-defined helicity, amphipathicity, and cationic charges, it readily binds to membranes and causes membrane change and disruption. This study provides details on how Aurein 1.2 interacts with charged lipid membranes by using neutron membrane diffraction (NMD) and neutron spin echo (NSE) spectroscopy on complex peptide-membrane systems. NMD provides higher resolution lipid bilayer structures than solution scattering. NMD revealed the peptide is mostly associated in the lipid headgroup region. Even at moderately high concentrations (e.g., peptide:lipid ratio of 1:30), aurein is located at the acyl chain-headgroup region without deep penetration into the hydrophobic acyl chain. However, it does reduce the elasticity of the membrane at that concentration, which was corroborated by the NSE results. Furthermore, NSE shows that aurein first softens the membrane, like other α-helical peptides at low concentration, but then makes the membrane much more rigid, even without membrane pore formation. The evidence shows that the action of aurein is quite strong for modifying charged lipid distribution without the need to form membrane pores or disintegrate membranes.

Keywords: antimicrobial peptide, membrane interaction, membrane modulus, neutron diffraction, neutron spin echo

Graphical Abstract

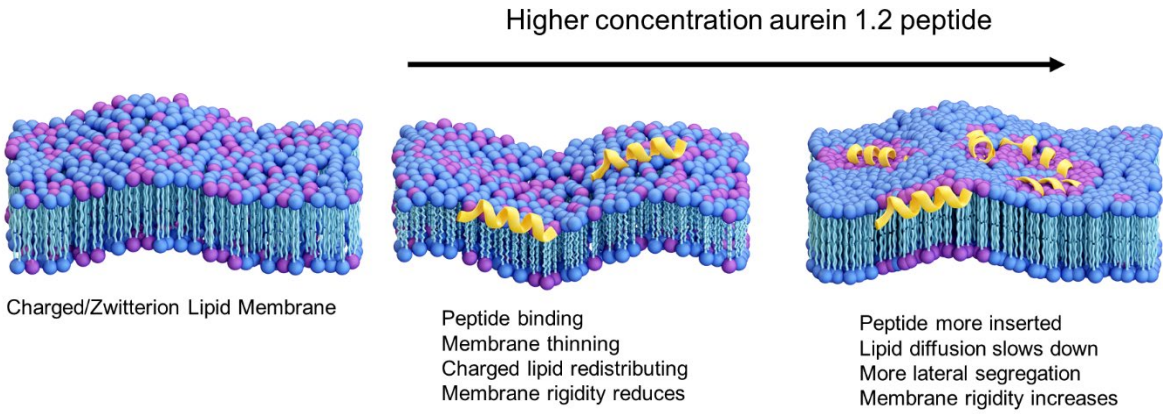

INTRODUCTION

Antimicrobial peptides (AMPs), found in all classes of life, are effective antibiotics that help the host defend against intruding bacteria. With relatively short sequences of a few dozen amino acids, they have a broad-spectrum effect against many pathogens, including viruses and cancerous cells. Their efficacy against different pathogens varies, but with the discovery of new AMPs from different species and de novo design, they can become effective therapeutic agents for ever increasing antibiotic crisis including multiple antibiotic-resistant bacteria [1]. Aurein 1.2 (aurein) is an efficacious AMP that has shown inhibition of Gram-negative and Gram-positive bacteria as well as moderate anti-cancer cell activity [2]. Originally discovered in the Australian Litoria frog genus, it has been studied to better understand the mechanism of AMP actions on membranes [2, 3] and inspired new peptide designs with enhanced antibacterial and antifungal activities [4–7].

Like many other AMPs, aurein is amphipathic and cationic. Driven by the electrostatic and hydrophobicity interaction, the peptide readily binds and interacts with lipid membranes, especially bacteria membranes in the presence of abundant negatively charged lipids and techoic acids in the Gram-positive bacteria peptidoglycan layer or with the lipopolysaccharide of the Gram-negative outer membrane [8–10]. The electrostatic interaction changes the delicate balance of the charged lipid allocation and dispersion in the membranes. In previous studies, aurein was found to be mostly on the surface of membranes [11–13]. The peptide causes the membrane thinning and eventually disintegrates a lipid membrane as peptide/lipid micelles detaching from the membrane in high concentrations [9]. Our previous study shows that aurein causes transbilayer asymmetry and lateral segregation or heterogeneity in binary lipid membranes that contain charged and zwitterionic lipids [14]. The peptide drives charged lipids to the outer leaflet even at low

concentration (peptide/lipid molar ratio (P/L) = 1/100) on the membrane. This effect is exacerbated at higher concentrations when the peptide orientation changes to the insertion state (i.e., perpendicular to the lipid membrane). This change of orientation is well understood for the two-state model because the hydrophobicity can drive an amphipathic peptide to form membrane pores or lipid-peptide super-molecular structures that cause cell lyses or disintegration of the cell membrane [15–17]. However, no membrane pores were detected with aurein in our previous studies, even at P/L = 1/10, whereas most peptides are in the inserted state, thereby implying that aurein is unable to make deep penetration [2]. Laterally on lipid membranes, the peptide promotes charged lipids into domain-like segregated structures, similar to the lipid gel phase caused by lowering the temperature. Studying the dynamics has shown that the rotational dynamics of the lipid are not altered significantly, but the lateral diffusion of the lipid is reduced, even at low peptide concentration, which is likely the cause of the lateral segregation that makes membranes more prone to defects and stresses [18]. Although many aurein activities are similar to other AMPs, its short length is intriguing, and its interaction with lipid layers still needs more understanding. These details are helpful in providing insight into the AMP mode of action. In this study, we further investigate how aurein interacts with charged lipid bilayers by using neutron membrane diffraction (NMD) and neutron spin echo (NSE) spectroscopy to understand how and where aurein is inserted into the lipid bilayer and how it affects the mechanical properties of membranes at different concentrations. Neutron is a nondestructive but sensitive probe for understanding lipid structures and dynamics [19–21]. The neutron scattering density profiles from NMD provide high-resolution information on lipid bilayers and structural change at different peptide concentrations [22–24]. The results show the membrane thinning effect like other membrane-active peptides. But at the two concentrations studied here (P/L= 1/100 and 1/30), aurein is not inserted into the acyl chain

region but always near the headgroup—between the inter-bilayer interfacial region and the acyl chain-headgroup region at different concentrations. In addition, we provide a detailed study of the collective nanosecond dynamics of the lipid bilayer composed of a zwitterionic lipid and a anionic lipid under the influence of aurein with NSE, which can be used to derive various elastic-mechanical properties, such as liposome and the bilayer bending moduli. The results show aurein softens the membrane at lower concentrations, but it can make the membrane more rigid without deep penetration or membrane pore formation at higher concentrations.

Our studies of the aurein peptide reveal details of a short yet potent AMP interaction with lipid membranes under various conditions. These insights on how a short peptide kills bacteria at low concentrations without forming pores or destroying membranes will be critical in designing and discovering more effective and economical AMPs.

MATERIALS AND METHODS

Neutron Membrane Diffraction Experiment

Aurein (>95% purity, GLFDIIKKIAESF-NH_2) was synthesized by GenScript USA Inc. (Piscataway, New Jersey, U.S.A). The 1,2-dimyristoyl-sn-glycero-3-phosphocholine (DMPC) and 1,2-dimyristoyl-sn-glycero-3-phospho-(1'-rac-glycerol) (DMPG) were purchased from Avanti Polar Lipids, Inc. in (Alabaster, Alabama, U.S.A.). All materials were used as delivered. The membrane thin film samples for NMD were prepared on 19 mm by 38 mm quartz substrates with aliquoted lipid/peptide in organic solvent using the established method [25]. Briefly, DMPC and DMPG were mixed as a 3:1 molar ratio in a solvent of trifluoroethanol: chloroform = 1:1 (v:v). The peptide was added with different P/L= 1/100 and 1/30. The solution was deposited on a quartz substrate. Before the samples were rehydrated with saturated D_2O vapor in a sealed jar at 40°C

overnight, they were placed in a constant airflow to allow the trace of organic solvent to dissipate completely. Visually, the membrane thin film was uniform and was used within 4 days of preparation for the neutron diffraction measurement. A total of two substrates with about 5 mg of lipid on each were stacked together for the experiment. A spacer made from aluminum foil was placed between the quartz substrates to allow quick changes of water vapor at different relative humidity (RH) levels during the experiment.

NMD measurements were performed using the Spallation Neutron Source's (SNS's) Extended Q-Range Small-Angle Neutron Scattering Diffractometer (EQ-SANS) at Oak Ridge National Laboratory (ORNL).[26] With a wavelength band of 2.6 to 6.2 Å selected from the chopper system and a sample-to-detector distance of 1.3 m, the time-of-flight for EQ-SANS provides good instrument resolution to cover an effective q-range of ~0.03 $Å^{-1}$ to 0.7 $Å^{-1}$ for the 1D diffraction pattern.

The NMD sample was housed in a sealed sample cell that separates the ambient atmosphere from the controlled ratio of H_2O/D_2O at desired RH and temperature throughout the experiment. The desired RH was provided by an RH generator (Model RH-200, L&C Science, Hialeah, Florida, USA) at RH 90%, 93%, and 97% (±1.8% for the uncertainty of the RH sensor). The RH generator's evaporator was fed by a water reservoir with the desired D_2O concentration of 8% (v/v). The humidified air flow rate was set to 500 cc per minute to allow the swift equilibrium of humidity and D_2O in the sample. The humidity change imposed on the samples does not alter the sample consistency because the same sample was used for the RH series.

Membrane Diffraction Data Collection and Reduction

Once sample was in equilibrium for an RH, the lamellar diffraction was collected by an oscillating ω scan, or *rocking scan*. The sample was rotated perpendicularly to its substrate surface around its center axis from ω = 0° to ~11° in steps of Δω = 0.1° for the same SNS proton charge count as the normalization standard at each step. Owing to the multiwavelength nature of the time-of-flight neutron instrument, the diffraction peaks in the raw detector were converted into Q space for integration. The data at each step were corrected for detector dark current, pixel sensitivity, and empty background using the facility-supplied Mantid (http://mantidproject.org/) reduction software and were translated to a 2D Qr-Qz map. The integrated intensity of each diffraction peak was obtained by summing the 2D map in Q space and analyzing it using routines implemented in MATLAB (MathWorks Inc., Natick, Massachusetts, USA). The diffraction amplitudes, $|F|$, obtained from the integrated diffraction peak intensity had to be corrected for the Lorentz factor, C_L; the absorption correction factor, C_{abs}; and the geometry correction factor, C_{geo} following Eq. (1) [23]:

$$|F| = \sqrt{I/I_0 C_L C_{abs} C_{geo}}, \quad (1)$$

where I_0 is the incident neutron flux, and Ω is the angular velocity of the scan. The Lorentz factor is given by

$$C_L = 1/\sin 2\theta, \quad (2)$$

where θ is the scattering angle. The absorption factor is given by

$$C_{abs} = \frac{(1-\exp(-2\mu d/sin\theta))}{2\mu d}, \quad (3)$$

where μ is the absorption coefficient of the sample, and d is the thickness of the sample. C_{geo} is a constant because the amount of sample immersed in the neutron beam remained approximately

unchanged for the angular range in the scans. The swelling method was used to solve the phases in the diffraction amplitudes, *F(h)* (see Figure S1 in Supporting Information) [27]. The neutron scattering length density (SLD) profile along the bilayer normal, $\rho(\mathrm{x})$, was constructed from *F(h)* by

$$\rho(\mathrm{x}) = \sum_h F(h)\cos(2\pi h\mathrm{x}/\mathrm{D}), \quad (4)$$

where h is the Miller index, and D is the repeating D-spacing. The SLD is normalized to the absolute scale by using the average SLD in a unit cell and the minimum point at the center of the unit cell where the terminal methyl group should be located. Details of the normalization are in the Supporting Information.

NSE Experiment

NSE spectra were measured using the SNS NSE instrument (BL-15) at ORNL [28]. The lipid vesicles with a concentration of 30 mg/mL in D_2O with two lipid compositions of different DMPC/DMPG = 3/1 and 1/1 in molar ratio were prepared using established methods [29,30]. Briefly, once lipids are mixed and suspended in solution with a few cycles of freeze and thaw, the extrusions were performed using a Avanti mini-extruder that was mounted on a Velmex linear motorized stage (Bloomfield, New York, USA) for 20 passes through the membrane with 0.1 μm-size holes. The peptide was titrated to the lipid solutions for different concentrations. The samples were loaded into 4 cm by 4 cm Hellma quartz cells with a beam path of 3mm. The samples were measured within 3 days of preparation, and the integrity of the samples were checked after the NSE experiment by small-angle x-ray scattering (SAXS) (Figure S2 in Supporting Information).

The samples were measured at 32°C controlled with a ThermoJet ES (SP Scientific, Warminster, Pennsylvania, USA) system with a precision of ±0.5°C. We chose two neutron

wavelength bands: 5–8 Å and 8–11 Å to cover Fourier times from approximately 0.07 to 100 ns and a Q range of approximately 0.045–0.125 $Å^{-1}$. The instrument resolution was measured with graphite and Al_2O_3 samples. To perform background subtraction, we also measured D_2O samples with the same sample cell geometry as the lipid solutions (4 cm by 4 cm by 3 mm). Data reduction was performed using the DrSPINE program [31].

NSE Data Analysis

According to Zilman and Granek [32], a freestanding single membrane fluctuation model was used to fit the intermediate scattering function *S(Q, t)/S(Q, 0)* as a Q · R >> 1 condition satisfied in the measurement, where *R* is the radius of the lipid vesicles:

$$\frac{S(Q,t)}{S(Q,0)} = e^{-(\Gamma(\mathrm{Q})\, t)^{\frac{2}{3}}}, \tag{5}$$

where *Q* and *t* are the wavenumber transfer and the Fourier time, respectively. From the fitting *Γ(Q)* (see Figure S3 in Supporting Information), the Q-dependent relaxation rate was obtained. The effective bending modulus $\tilde{\kappa}$ can be obtained by the equation from Watson and Brown [33]:

$$\Gamma(\mathrm{Q}) = 0.025\, \gamma \sqrt{\frac{k_B T}{\tilde{\kappa}}} \frac{k_B T}{\eta_{D_2O}} Q^3, \tag{6}$$

where γ is assumed to be 1 when $\tilde{\kappa} \gg k_B T$, which is typical for lipid bilayers near room temperature [21,32], and $\eta_{D_2O} = 0.9318\ cP$ is the viscosity of D_2O at 32°C according to the data found in the literature [34]. There is a debate in the literature, e.g., [21,35,36] about the numerical pre-factor in the above equation. We keep it at 0.025 in accordance with the original paper by Watson and Brown.

From $\tilde{\kappa}$, the intrinsic bending modulus, κ, reflecting the dynamics of a bilayer can be derived from

$$\tilde{\kappa} = \kappa\left[1 + 48\left(\frac{h}{2h_c}\right)^2\right], \quad (7)$$

where h is the height of the neutral surface from the bilayer midplane, and h_c is the monolayer hydrocarbon thickness. The ratio $\frac{h}{2h_c}$ cannot be measured experimentally, and the ranges differ in the literature. We follow Nagao et al. [21] and use $\frac{h}{2h_c} = 0.5$. The bilayer area's compressibility modulus, K_A, can be deduced from κ with the assumption of the thin elastic sheet as the bending fluctuation leads one leaflet to stretch with the other leaflet compressing [21]:

$$K_A = \frac{\beta\kappa}{(2h_c)^2}, \quad (8)$$

where β is the coupling constant between the two leaflets ranging from 12 (fully coupled) to 48 (completely uncoupled). Here we use 24 to represent a condition in between [37]. The values of h_c are from previous results of small-angle neutron scattering (SANS) [14].

RESULTS AND DISCUSSION

Membrane Structure Changes from the Membrane Diffraction Results

Samples with a single lipid composition of DMPC/DMPG = 3/1 with the lipid-only sample and P/L = 1/100 and 1/30 were measured. All samples showed good lamellar diffraction with at least four orders of diffraction peaks. There was no sign of additional peaks outside the lamellar diffraction, thereby indicating no correlation of in-plane features for the multi-lamellar samples at all peptide concentrations and RH conditions. From this data, the averaged 1D structural profile

normal to the membrane can be obtained but not the lateral segregation of lipids within the membrane plane. The diffraction amplitudes and phases derived from the diffraction data and the swelling method are presented in Table 1. Note that we did not collect the data for P/L = 1/100 at RH 97% owing to availability of the allocated neutron beam line; however, this does not affect the data analysis and the completeness of the study as the trend of changes in other conditions with all samples is sufficient for analysis.

Table 1. Diffraction amplitudes (arbitrary unit) and phases. Only four orders of diffraction peaks were used because the fifth order is very weak in intensity.

		Lipid-only			**P/L = 1/100**		**P/L = 1/30**		
	phase	RH	RH	RH	RH	RH	RH	RH	RH
F(1)	−1	18.5	19.6	24.2	21.9	17.6	32.4	33.6	33.9
F(2)	−1	9.5	9.2	8.2	12.6	11.4	14.0	12.5	11.9
F(3)	+1	10.0	9.8	9.7	11.7	10.5	12.2	11.8	11.6
F(4)	−1	10.2	9.8	10.1	11.1	10.5	10.5	10.1	10.2

Table 2. D-spacing/the peak-to-peak (P-P) distance and the peak height for different P/L ratios at different humidity levels (Å).

	Lipid-only			***P/L = 1/100***			***P/L = 1/30***		
RH	D-spacing (Å)	P-P distance (Å)	Peak height (fm/Å^3)	D-spacing (Å)	P-P distance (Å)	Peak height (fm/Å^3)	D-spacing (Å)	P-P distance (Å)	Peak height (fm/Å^3)
97%	46.68±0.25	33.38±0.18	0.1714	N/A	N/A	N/A	41.78±0.22	29.84±0.16	0.1674
93%	46.28±0.20	33.18±0.15	0.1689	43.94±0.20	31.24±0.14	0.1717	41.42±0.21	29.80±0.15	0.1674
90%	46.10±0.20	33.42±0.15	0.1633	43.80±0.19	31.08±0.14	0.1752	41.30±0.20	29.80±0.14	0.1675

From the peak positions on the membrane diffraction pattern, D-spacings—the 1D unit cell lattice sizes normal to the bilayer—were obtained from peak position Q_{peak} by $D = 2\pi/Q_{peak}$ (Table 2). The data show that D-spacing decreases gradually with decreasing RH. For example, for the lipid-only sample, its D-spacing changed from 46.68 Å at 97% RH to 46.10 Å at 90% RH. In contrast, the headgroup P-P distance (Table 2), which is a more accurate indicator of bilayer thickness, remained more or less the same in the same sample, regardless of the RH. The peaks are from the phosphate group of both DMPC and DMPG with much higher SLD density in neutron scattering as maxima in the reconstructed profiles (Figure 1). The reduction in D-spacing is explained well by the reduction of the water layer between the lipid bilayers because the water molecules are being removed with decreasing RH. The bilayer thickness measured by the P-P distance remained the same, which shows the lipid bilayer is relatively stable in the lamellar phase at different osmotic pressures exerted by RH [38]. In contrast, D-spacing and P-P distance both changed substantially when aurein was added (e.g., at RH 93%); the D-spacing changed from 46.28 Å in the lipid-only samples to 43.94 Å (P/L = 1/100) and 41.42 Å (P/L = 1/30). At the same time, P-P changes from 33.18 Å in the lipid-only sample to 31.24 Å (P/L = 1/100) and 29.80 Å (P/L = 1/30). Data from other RH levels show a similar trend. It is evident that aurein binds to the membrane surface with a strong thinning effect even at the low concentration of P/L=1/100. The membrane thinning is also consistent with observations made from the DMPC/DMPG vesicle SANS experiment in solution but to a larger degree [14]. For example, at 97% RH, the P-P in the P/L=1/30 sample was reduced by 3.5 Å compared to the lipid-only sample at 97% RH. In solution experiment, the decrease was about 1 Å, much smaller, because the sample in solution was much more swelled in water.

The SLD profiles provide more detailed structural insight into how aurein modifies the bilayer. The measurement was performed with 8% D_2O. The SLD of the water (8% D_2O) is zero because the negative scattering length from the protiated hydrogen cancels out that of deuterium and oxygen. This ensures that the contribution of hydration water to the SLD profile is avoided to provide less ambiguity in the interpretation of the structure of the lipid bilayer and peptide complex [24].

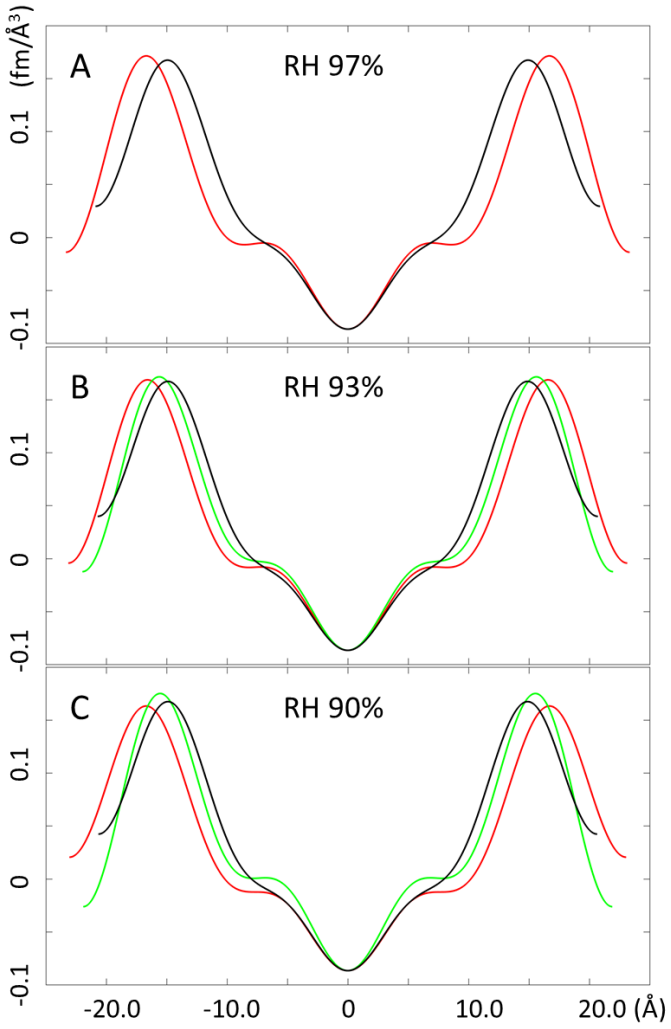

Figure 1. Reconstructed SLD structure profiles at different RH levels.

With the addition of peptide, if its SLD is significantly different from lipid SLD, the change in the overall profile can be used to pinpoint the peptide location [24,39,40]. However, in this case, aurein SLD is ~0.1768 fm/Å^3 at 8% D_2O (see Table S1 in Supporting Information), which is lower than the average SLD of the headgroup of the DMPC/DMPG mixture (~0.21 fm/Å^3). The location of aurein cannot be determined by subtracting the lipid-only SLD profile from the peptide-containing samples because the addition of peptide does not increase the SLD. From the normalized SLD profile, the peak maxima are between 0.1633 and 0.1752 fm/Å^3, which is lower than the calculated average SLD of the DMPC/DMPG headgroup mixture and aurein. This indicates that at least 2–3 water molecules are associated with each headgroup on average, bringing the SLD down to ~0.17 fm/Å^3.

The region between the inter-bilayer space, for example, near the end of the SLD profiles at ~ ±20 Å, provides additional clues on how peptide changes the bilayer at its water-headgroup interface. At 93% RH (Figure 1[B]), the SLD change is insignificant with both the lipid-only sample and the P/L=1/100 sample close to 0 fm/Å^3 around the region. The slight decrease in P/L = 1/100 can be attributed to more water molecules penetrating into the adjacent volume as the peptide starts to perturb the water-headgroup interface. The SLD change from peptide binding and water penetration is mostly cancelled out. However, at P/L = 1/30, the SLD change from peptide binding is much higher owing to much more peptide binding to the headgroup than the penetration of additional water molecules, thereby bringing the SLD to ~0.04 fm/Å^3, as shown in the SLD profile (Figure 1[B]). The trend is the same at 90% RH, but the initial decrease of SLD is more significant at the low peptide concentration (P/L = 1/100) (Figure 1[C]), likely due to water molecules in the system being less available at lower humidity. At 97% RH, the higher peptide concentration (P/L = 1/30) also resulted in a higher SLD near the headgroup with presumably more

peptide binding than water penetration into headgroup (Figure 1[A]). The SLD change at different P/L ratios indicates aurein is associated with the headgroup. The peptide binding initially promotes water penetration but outcompetes it with an increasing peptide concentration. No larger water penetration or peptide poration is suggested by the results, and this is corroborated by our previous studies, in which no membrane pore formation was observed, even at higher concentrations of aurein [14].

For the lipid-only sample, while P-P distance holds steady at different RH levels, the headgroup-peak SLD maxima decreases slightly with decreasing RH levels (Table 2). Interestingly, at P/L = 1/30, which is a relatively high concentration, the P-P distance and the headgroup peak height hold constant with RH change. For P:L = 1:100, the peak height increases slightly from 93% RH to 90% RH. Decreasing RH levels is the equivalent of applying higher osmotic pressure on the membrane [38,41], and the pressure exerted will stretch or compress the bilayer to cause the volume to change for different components, such as the headgroup, ester backbone, and acyl chain, which causes the change in SLD peaks. But the pressure effect is void in samples with relatively high peptide concentration. The unchanged peak height in the P/L = 1/30 sample suggests that once a certain amount of peptide binds to the lipid, the elasticity of the lipid bilayer is reduced. In other words, the bilayer is less stretchable or is in a more rigid state. This corroborates the NSE observation presented in the next section. Our previous dynamics study showed that aurein restricts the lipid lateral motion in the lipid fluid phase even at low aurein concentrations. The structure results here indicate that the restraint by aurein does indeed change the lipid bilayer's response to external force.

At P/L = 1/30, the profiles also show significant change in the intra-bilayer SLD, as the shoulder peaks between the headgroup disappear as P-P distance is reduced with peptide binding.

Most importantly, the lack of increase in SLD around the acyl chain indicates aurein is not penetrating deeply into the chain region. Based on this result, the aurein distribution is likely still between the water-headgroup and the chain-headgroup interfaces.

The Membrane Rigidity Change Revealed by Neutron Spin Echo

The NSE experiment was performed on lipid vesicle solution samples similar to those used in the SANS experiment previously but at higher concentrations to improve the signal. Because the measurement for each sample took about 24–48 hours, all samples were checked by SAXS after the experiment. The SAXS data showed the lipid bilayer and unilamellarity was well kept (Figure S2). In addition, the shifting of first minima between 0.03 and 0.04 $Å^{-1}$, with peaks of higher Q as the peptide concentration increases in both DMPC/DMPG = 3/1 and 1/1 samples, verified that aurein binding to the membrane is a signature of membrane thinning [42]. The intermediate structure function, *S(Q, t) / S(Q, 0)*, from the NSE measurement fit well with the exponential form of Zilman and Granek for all samples (Figure S3 in Supporting Information) [32]. From the fitting, the Q-dependent relaxation rate of $\Gamma(Q) / Q^3$ vs. Q was shown in Figure 2. All samples showed a similar trend from a Q range of 0.03 to 0.11 $Å^{-1}$ above the length scale of the bilayer thickness. With the averaged $\Gamma(Q) / Q^3$ over the Q range measured from 0.0033 to 0.122 $Å^{-1}$ (Table 3), the effect of aurein on both lipid compositions was similar: at the lower aurein concentration (P/L = 1/100), $\Gamma(Q) / Q^3$ increases slightly from the lipid-only bilayer; but at the higher aurein concentration (P/L = 1/30), it decreases to be smaller than the lipid-only bilayer.

From $\Gamma(Q)/Q^3$ and additional structural parameters, the effective bending modulus, $\tilde{\kappa}$; the intrinsic bending modulus, κ; and the bilayer area compressibility modulus, K_A are derived to describe the overall dynamics of lipid bilayer vesicles, the dynamics of the lipid bilayer, and the

lipid bilayer area compressibility, respectively. From the results in Table 3, for both lipid compositions, the addition of aurein lowers all of moduli, which indicates reduced rigidity at P/L = 1/100. However, at the higher peptide concentration (P/L = 1/30) the moduli are increased with the rigidity beyond the peptide-free samples (e.g., Figure 3).

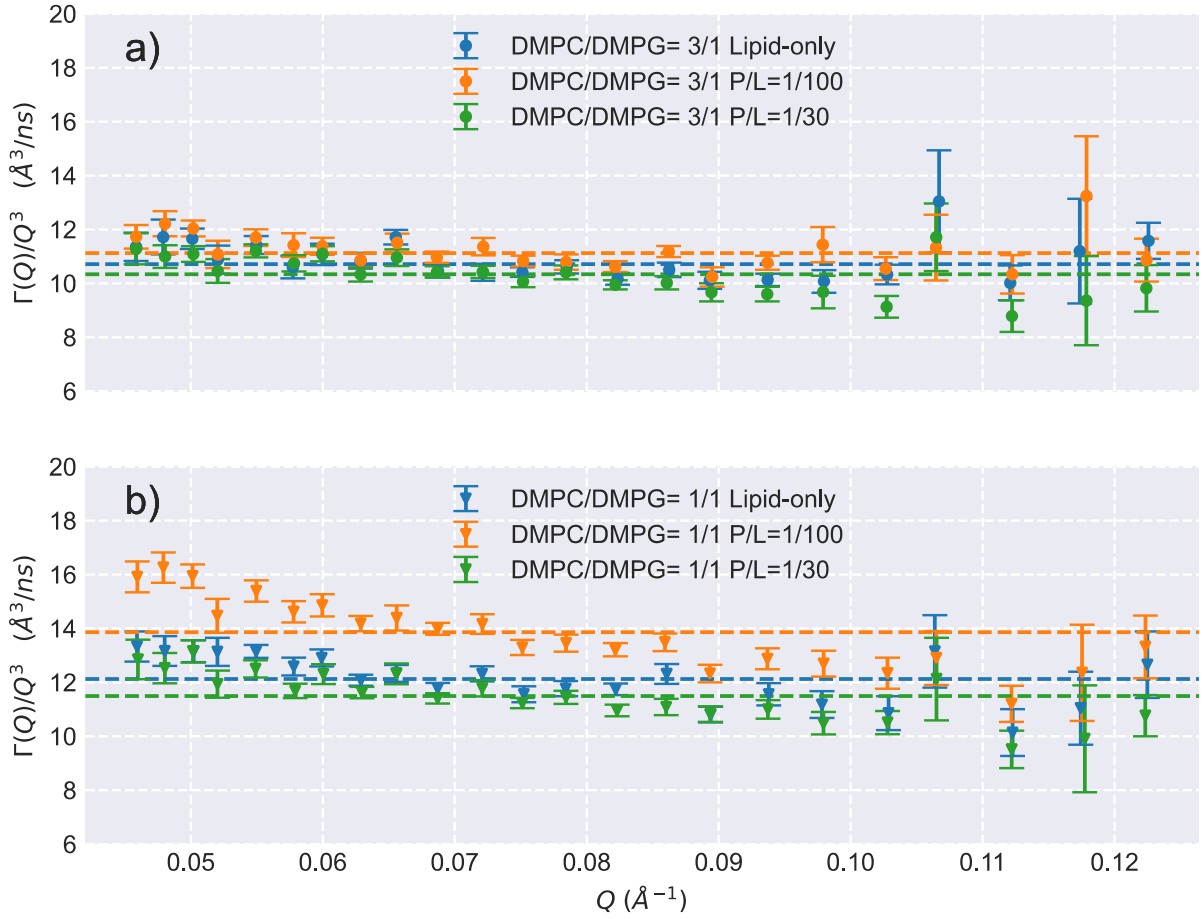

Figure 2. The Q-dependent relaxation rate Γ(Q) / Q^3 vs. Q for DMPC/DMPG = 3/1 and 1/1 samples with various aurein concentrations (lipid-only, P/L = 1/100, P/L = 1/30). The dash lines are the averaged values from the measured Q range.

Table 3. Averaged values of Γ/Q^3 from the measured Q range, the effective bending modulus, $\tilde{\kappa}$, the intrinsic bending modulus, κ, and the bilayer area compressibility modulus, K_A.

Sample	$\Gamma(Q)/Q^3$ ($Å^3$/ns)	$\tilde{\kappa}$ (k_BT)	$\kappa(k_BT)$	K_A (mN/m)
DMPC/DMPG =3/1 lipid-only	10.7 ± 0.6	112± 13	8.6 ± 0.9	26.2 ± 2.9
P/L=100	11.1 ± 0.5	104 ± 9	8.0 ± 0.7	24.8 ± 2.2
P/L=30	10.3 ± 0.6	120 ± 14	9.3 ± 1.1	28.4 ± 3.3
DMPC/DMPG =1/1 lipid-only	12.1 ± 0.8	87 ± 12	6.7 ± 0.9	26.7 ± 3.5
P/L=100	13.9 ± 1.2	66 ± 11	5.1 ± 0.9	20.4 ± 3.5
P/L=30	11.5 ± 0.7	97 ± 12	7.4 ± 0.9	27.4 ± 3.3

Lipid vesicles and the bilayer mixed with charged/zwitterion lipids are less rigid than lipid vesicles made of a single zwitterion lipid (e.g., DMPC) [43–45]. Our results from the lipid-only samples are consistent with this assertion because both lipid compositions used here showed much lower rigidity when compared to DMPC vesicles measured by NSE [21]. Moreover, the rigidity change caused by aurein was more prominent in the composition with a more charged lipid, as indicated by the magnitude of changes in DMPC/DMPG = 1/1 being higher than the changes with DMPC/DMPG = 3/1 at the peptide concentrations used (Figure 3). Therefore, lipid composition with a charged lipid plays a role in magnifying the peptide's effect because the increasing inhomogeneity of charged/zwitterion lipid mixture towards lateral phase segregation is promoted by the addution of aurein [46]. This can be another reason that membranes with a higher ratio of charged lipids are more prone to membrane-active peptides in addition to higher electrostatic interaction.

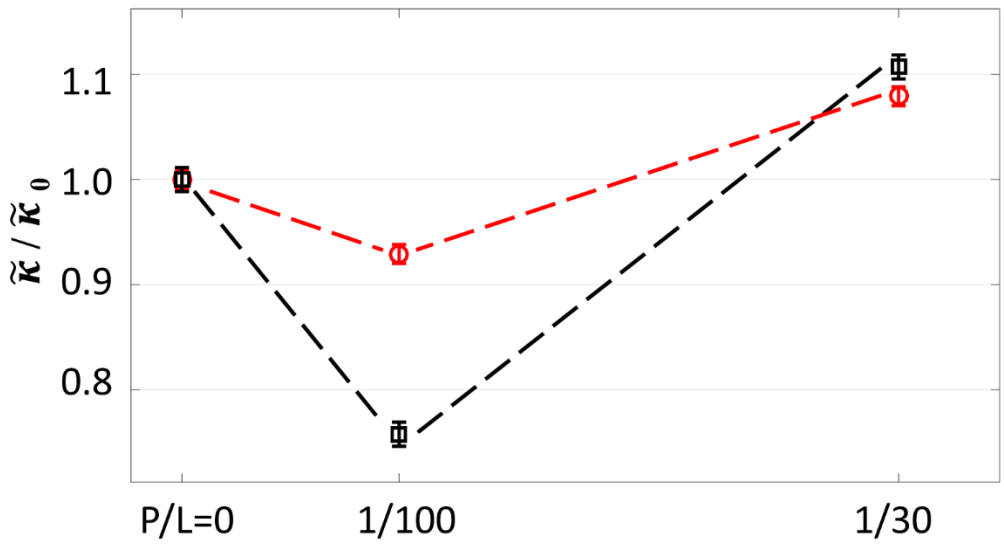

Figure 3 The relative ratio of effective bending moduli $\tilde{\kappa}$ to the lipid-only samples (Red: DMPC/DMPG = 3/1; Black: DMPC/DMPG = 1/1; the dash lines are for guiding eyes only)

For both lipid compositions, initially the low peptide concentration (P/L = 1/100) reduces the membrane rigidity shown by various bending moduli (Table 3, Figure 3). The decrease is then reversed at the higher peptide concentration (P/L = 1/30) with a significant increase in bending moduli beyond the lipid-only samples. Previous studies on membrane mechanical properties using NSE have shown that membrane active peptides with a β secondary structure (e.g., gp41rk [43], gramicidin [47], Amyloid-β peptide [48]), make the membrane more rigid as they are likely to increase the acyl chain order. For the α-helical membrane-active peptide, the change is more complex. For example, alamethicin was found to increase lipid chain disorderness and soften membranes with single-composition zwitterion lipids throughout different P/L concentrations, but the change is more prominent at lower concentrations [47,49–51]. Melittin, another well-studied α-helical peptide, decreases the intrinsic bending modulus and the bilayer compressibility modulus of DOPC vesicles below P/L = 1/250 and significantly increases them—compared with the lipid-

only sample—above P/L = 1/50 [49]. The melittin study attributes the increase in rigidity to the repulsive interpore correlation posed by melittin-membrane pore formation [49]. As a short α-helical peptide, aurein's dual action on the membrane's overall mechanical properties for both softening and rigidifying are intriguing. In our previous experiment with oriented circular dichroism on the multi-lamellar samples with the same DMPC/DMPG compositions, aurein was found to be in the surface binding mode, and the peptide is parallel to the surface bilayer at P/L = 1/100. Even at P/L = 1/30, the majority of the peptide is still in the parallel surface state. Only at higher concentrations (e.g., P/L = 1/10) does a significant amount of the peptide change orientation to be perpendicular to membranes [14]. Also, no transmembrane pore was found in this state. Although the insertion into the acyl chain is limited, it is possible that a slightly deeper penetration of aurein into the acyl chain-headgroup interface can induce more order and rigidify the membrane. This possibility is also reflected by the NMD result presented here because the lipid-only and P/L = 1/100 samples show notable changes in P-P distance and headgroup peak height with RH change, but those in the P/L = 1/30 sample were unaffected once more insertion of aurein reduced the membrane elasticity.

Discussion on the Mode of Action

As a α-helical membrane-active AMP, aurein is one of the shortest found in nature, with only 13 amino acids. Structurally, it is well defined with high helicity and amphipathicity and includes a number of charges. With those characteristics, and as shown in a number of previous studies, it is efficient and effective at attacking anionic membranes in bacteria [2,52,53]. Our series of structural and dynamical studies on aurein revealed many more details on its interaction with different membranes. In solution (SANS and SAXS) and substrate-supported model membranes (NMD), aurein readily binds to membranes with and without negatively charged lipids to exert a

membrane-thinning effect like many other membrane-active peptides. The electrostatic interaction and hydrophobicity play roles in the binding [52,54]. The binding causes significant asymmetry in charged lipid distribution across the leaflets of the bilayer and lateral segregation in the membrane plane [14]. This indicates that aurein promotes heterogeneity in a charged/zwitterion lipid mixture. In the much smaller length scale of individual lipids, the addition of aurein always reduces the lateral diffusion motion without affecting the internal motion of the individual lipid [55]. At larger scales, the bending fluctuation and compressibility from the collective motion of lipids can be modified more delicately by using peptide binding: at low concentrations, aurein softens membranes; at higher concentrations, it will stiffen membranes. This points to a change of interaction when the peptide is at a higher concentration. We know aurein will become perpendicular to the membrane at very high concentration (e.g., P/L = 1/10), in which the insertion into the acyl chain can line up along the chain to stiffen the membrane like other peptides (e.g., melittin), even without pore formation. But at a moderately high concentration (e.g., P/L = 1/30), the peptide parallel to the surface with slightly more penetration in the acyl chain-headgroup region but not necessarily deep into the chain can still stiffen the membrane, as shown by the NMD and NSE results. In contrast, at low concentrations (e.g., P/L = 1/100), the peptide insertion is shallower and sporadic. The softening from the perturbation of aurein binding is more or less similar to that of other helical membrane-active peptides at low concentration [49,50]. Regardless softening or stiffening, the peptide changes membrane properties more signficantly at a higher charged/zwitterion lipid ratio. Also, hydrophobic mismatches between the acyl chains of different lipid components as they associated with different numbers of peptides can also cause lateral phase segregation [46]. Additionally, the dimerization or oligomerization of aurein can also play a role in enhancing the interaction because the dimerization effectively

increases the volume of aurein in perturbation [52,54,56]. All of those factors combined suggest how delicate the interaction of a peptide and a membrane can be, especially with a short yet very potent membrane-active peptide on membranes with charged lipids.

The evidence shows that the action of aurein is quite strong for modifying charged lipid distribution without the need to form membrane pores or disintegrate membranes. Aurein changes a membrane's mechanical properties, and this action is more drastic when a membrane has charged lipid with reduced lateral lipid diffusion. When the overall heterogeneity increases, especially, if the cationic peptide associates more with the laterally segregated anionic lipid, the uneven distribution can promote patches of more rigid domains with a coexistence of the much less rigid region. However, these increases in rigidity by segregation do not necessarily protect the membrane from disruption: the boundary between them makes the membrane more fragile because the mismatch of the modulus and thickness can become the breaking point when under stress. The change in the localized rigidity can also disturb other membrane-associated molecules (e.g., proteins) out their normal functional environment.

CONCLUSIONS

In this study, we further surveyed aurein's mode of action on membranes with charged lipids by using NMD and NSE to find changes in the membrane structure and mechanical properties, respectively. The NMD results revealed membrane thinning consistent with previous experiments with other membrane-active peptides. At the two concentrations we studied (P/L = 1/100 and P:L = 1/30), the peptides were mostly associated in the lipid headgroup region. The peptide at P/L = 1/30 penetrated the acyl chain-headgroup but not deep into the hydrophobic acyl chain region. The NSE shows aurein first softened the membrane like other α-helical

peptides but then made the membrane much more rigid without deep penetration or membrane pore formation.

The results provide a detailed picture of the interaction between a membrane-active peptide and more sophisticated model membranes with charged and zwitterionic lipids. The interaction is more intricate than many existing models, even in the case of a small and relatively simple α-helical peptide. The membrane modifications caused by peptides can be very delicate depending on the relative strength of different factors, which are likely determined by the peptide sequence and lipid properties. A detailed understanding of these factors is imperative to precisely control or modulate the interaction when improving the performance of AMPs.

ASSOCIATED CONTENT

Supporting Information.

The additional figures and table are available free of charge in the Supporting Information on publication website.

Notes

The authors declare no competing financial interests.

ACKNOWLEDGMENTS

The SNS, where EQ-SANS and NSE are located, is supported by U.S. Department of Energy's (DOE) Scientific User Facilities Division, Office of Basic Energy Sciences. S. Q. was

partly supported by the Center for Structural Molecular Biology, a user facility funded by DOE's Office of Biological and Environmental Research. S. Q. was partly supported in this research by resources of the SNS Second Target Station Project at ORNL. The D_2O used in this research was supplied by the DOE's Isotope Program in the Office of Nuclear Physics. ORNL is managed by UT-Battelle LLC for DOE's Office of Science.

REFERENCES

[1] H.-K. Kang, C. Kim, C.H. Seo, Y. Park, The therapeutic applications of antimicrobial peptides (AMPs): a patent review, J Microbiol., 55 (2017) 1–12.
[2] S. Zhu, M.-A. Sani, F. Separovic, Interaction of cationic antimicrobial peptides from Australian frogs with lipid membranes, Peptide Science, 110 (2018) e24061.
[3] J.E. Nielsen, V.A. Bjørnestad, V. Pipich, H. Jenssen, R. Lund, Beyond structural models for the mode of action: How natural antimicrobial peptides affect lipid transport, Journal of Colloid and Interface Science, 582 (2021) 793–802.
[4] M.-R. Lee, N. Raman, S.H. Gellman, D.M. Lynn, S.P. Palecek, Incorporation of β-Amino Acids Enhances the Antifungal Activity and Selectivity of the Helical Antimicrobial Peptide Aurein 12, ACS Chem. Biol., 12 (2017) 2975–2980.
[5] N. Klubthawee, P. Adisakwattana, W. Hanpithakpong, S. Somsri, R. Aunpad, A novel, rationally designed, hybrid antimicrobial peptide, inspired by cathelicidin and aurein, exhibits membrane-active mechanisms against Pseudomonas aeruginosa, Sci Rep, 10 (2020) 9117.
[6] M. Ramezanzadeh, N. Saeedi, E. Mesbahfar, P. Farrokh, F. Salimi, A. Rezaei, Design and characterization of new antimicrobial peptides derived from aurein 12 with enhanced antibacterial activity, Biochimie, 181 (2021) 42–51.
[7] X. Li, Y. Li, A. Peterkofsky, G. Wang, NMR studies of aurein 12 analogs, Biochimica et Biophysica Acta (BBA) - Biomembranes, 1758 (2006) 1203–1214.
[8] E.E. Ambroggio, F. Separovic, J.H. Bowie, G.D. Fidelio, L.A. Bagatolli, Direct Visualization of Membrane Leakage Induced by the Antibiotic Peptides: Maculatin, Citropin, and Aurein, Biophysical Journal, 89 (2005) 1874–1881.
[9] M. Shahmiri, M. Enciso, A. Mechler, Controls and constrains of the membrane disrupting action of Aurein 12, Scientific Reports, 5 (2015) 16378.
[10] M. Laadhari, A.A. Arnold, A.E. Gravel, F. Separovic, I. Marcotte, Interaction of the antimicrobial peptides caerin 11 and aurein 12 with intact bacteria by 2H solid-state NMR, Biochimica et Biophysica Acta (BBA) - Biomembranes, 1858 (2016) 2959–2964.
[11] D.I. Fernandez, A.P.L. Brun, T.C. Whitwell, M.-A. Sani, M. James, F. Separovic, The antimicrobial peptide aurein 12 disrupts model membranes via the carpet mechanism, Phys. Chem. Chem. Phys., 14 (2012) 15739–15751.
[12] T.-H. Lee, C. Heng, M.J. Swann, J.D. Gehman, F. Separovic, M.-I. Aguilar, Real-time quantitative analysis of lipid disordering by aurein 12 during membrane adsorption, destabilisation and lysis, Biochimica et Biophysica Acta (BBA) - Biomembranes, 1798 (2010) 1977–1986.

[13] A. Mechler, S. Praporski, K. Atmuri, M. Boland, F. Separovic, L.L. Martin, Specific and selective peptide-membrane interactions revealed using quartz crystal microbalance, Biophys. J., 93 (2007) 3907–3916.
[14] D.K. Rai, S. Qian, Interaction of the Antimicrobial Peptide Aurein 12 and Charged Lipid Bilayer, Scientific Reports, 7 (2017) 3719.
[15] H.W. Huang, Action of Antimicrobial Peptides: Two-State Model, Biochemistry, 39 (2000) 8347–8352.
[16] S. Qian, W. Wang, L. Yang, H.W. Huang, Structure of transmembrane pore induced by Bax-derived peptide: Evidence for lipidic pores, Proceedings of the National Academy of Sciences, 105 (2008) 17379–17383.
[17] S. Qian, W. Wang, L. Yang, H.W. Huang, Structure of the Alamethicin Pore Reconstructed by X-Ray Diffraction Analysis, Biophysical Journal, 94 (2008) 3512–3522.
[18] R.M. Epand, R.F. Epand, Lipid domains in bacterial membranes and the action of antimicrobial agents, Biochimica et Biophysica Acta (BBA) - Biomembranes, 1788 (2009) 289–294.
[19] S. Qian, V.K. Sharma, L.A. Clifton, Understanding the Structure and Dynamics of Complex Biomembrane Interactions by Neutron Scattering Techniques, Langmuir, (2020).
[20] J.D. Nickels, S. Chatterjee, C.B. Stanley, S. Qian, X. Cheng, D.A.A. Myles, R.F. Standaert, J.G. Elkins, J. Katsaras, The in vivo structure of biological membranes and evidence for lipid domains, PLOS Biology, 15 (2017) e2002214.
[21] M. Nagao, E.G. Kelley, R. Ashkar, R. Bradbury, P.D. Butler, Probing Elastic and Viscous Properties of Phospholipid Bilayers Using Neutron Spin Echo Spectroscopy, J. Phys. Chem. Lett., 8 (2017) 4679–4684.
[22] S. Qian, D.K. Rai, Grazing-Angle Neutron Diffraction Study of the Water Distribution in Membrane Hemifusion: From the Lamellar to Rhombohedral Phase, J. Phys. Chem. Lett., 9 (2018) 5778–5784.
[23] L. Ding, T.M. Weiss, G. Fragneto, W. Liu, L. Yang, H.W. Huang, Distorted Hexagonal Phase Studied by Neutron Diffraction: Lipid Components Demixed in a Bent Monolayer, Langmuir, 21 (2005) 203–210.
[24] X. Chen, F. Sa'adedin, B. Deme, P. Rao, J. Bradshaw, Insertion of TAT peptide and perturbation of negatively charged model phospholipid bilayer revealed by neutron diffraction, Biochimica et Biophysica Acta (BBA) - Biomembranes, 1828 (2013) 1982–1988.
[25] D. Pan, W. Wang, W. Liu, L. Yang, H.W. Huang, Chain Packing in the Inverted Hexagonal Phase of Phospholipids: A Study by X-ray Anomalous Diffraction on Bromine-labeled Chains, J. Am. Chem. Soc., 128 (2006) 3800–3807.
[26] W.T. Heller, V.S. Urban, G.W. Lynn, K.L. Weiss, H.M. O'Neill, S.V. Pingali, S. Qian, K.C. Littrell, Y.B. Melnichenko, M.V. Buchanan, D.L. Selby, G.D. Wignall, P.D. Butler, D.A. Myles, The Bio-SANS instrument at the High Flux Isotope Reactor of Oak Ridge National Laboratory, Journal of Applied Crystallography, 47 (2014) 1238–1246.
[27] S.L. Bragg, F.R. S, M.F. Perutz, The structure of haemoglobin, Proc. R. Soc. Lond. A, 213 (1952) 425–435.
[28] M. Ohl, M. Monkenbusch, N. Arend, T. Kozielewski, G. Vehres, C. Tiemann, M. Butzek, H. Soltner, U. Giesen, R. Achten, H. Stelzer, B. Lindenau, A. Budwig, H. Kleines, M. Drochner, P. Kaemmerling, M. Wagener, R. Möller, E.B. Iverson, M. Sharp, et al., The spin-echo spectrometer at the Spallation Neutron Source (SNS), Nuclear Instruments and Methods in

Physics Research Section A: Accelerators, Spectrometers, Detectors and Associated Equipment, 696 (2012) 85–99.
[29] S. Qian, W.T. Heller, Peptide-Induced Asymmetric Distribution of Charged Lipids in a Vesicle Bilayer Revealed by Small-Angle Neutron Scattering, J. Phys. Chem. B, 115 (2011) 9831–9837.
[30] S. Qian, W.T. Heller, Melittin-induced cholesterol reorganization in lipid bilayer membranes, Biochimica et Biophysica Acta (BBA) - Biomembranes, 1848 (2015) 2253–2260.
[31] P.A. Zolnierczuk, O. Holderer, S. Pasini, T. Kozielewski, L.R. Stingaciu, M. Monkenbusch, Efficient data extraction from neutron time-of-flight spin-echo raw data, J Appl Cryst, 52 (2019) 1022–1034.
[32] A.G. Zilman, R. Granek, Undulations and Dynamic Structure Factor of Membranes, Phys. Rev. Lett., 77 (1996) 4788–4791.
[33] M.C. Watson, F.L.H. Brown, Interpreting Membrane Scattering Experiments at the Mesoscale: The Contribution of Dissipation within the Bilayer, Biophysical Journal, 98 (2010) L9–L11.
[34] R. Hardy, R.L. Cottington, Viscosity of deuterium oxide and water in the range 5 to 125 C, (1949).
[35] S. Gupta, J.U. De Mel, G.J. Schneider, Dynamics of liposomes in the fluid phase, Current Opinion in Colloid & Interface Science, 42 (2019) 121–136.
[36] I. Hoffmann, Data Analysis and Background Subtraction in Neutron Spin Echo Spectroscopy, Frontiers in Physics, 8 (2021) 602.
[37] W. Rawicz, K.C. Olbrich, T. McIntosh, D. Needham, E. Evans, Effect of Chain Length and Unsaturation on Elasticity of Lipid Bilayers, Biophysical Journal, 79 (2000) 328–339.
[38] J. Milhaud, New insights into water–phospholipid model membrane interactions, Biochimica et Biophysica Acta (BBA) - Biomembranes, 1663 (2004) 19–51.
[39] F. Foglia, M.J. Lawrence, B. Demeė, G. Fragneto, D. Barlow, Neutron diffraction studies of the interaction between amphotericin B and lipid-sterol model membranes, Scientific Reports, 2 (2012).
[40] S.H. White, G.I. King, J.E. Cain, Location of hexane in lipid bilayers determined by neutron diffraction, Nature, 290 (1981) 161–163.
[41] S. Qian, H.W. Huang, A Novel Phase of Compressed Bilayers That Models the Prestalk Transition State of Membrane Fusion, Biophysical Journal, 102 (2012) 48–55.
[42] H.W. Huang, F.-Y. Chen, M.-T. Lee, Molecular Mechanism of Peptide-Induced Pores in Membranes, Phys. Rev. Lett., 92 (2004) 198304.
[43] W.T. Heller, P.A. Zolnierczuk, The helix-to-sheet transition of an HIV-1 fusion peptide derivative changes the mechanical properties of lipid bilayer membranes, Biochimica et Biophysica Acta (BBA) - Biomembranes, 1861 (2019) 565–572.
[44] Y. Takechi-Haraya, Y. Goda, K. Sakai-Kato, Atomic Force Microscopy Study on the Stiffness of Nanosized Liposomes Containing Charged Lipids, Langmuir, 34 (2018) 7805–7812.
[45] S.K. Saha, S.U. Alam Shibly, M. Yamazaki, Membrane Tension in Negatively Charged Lipid Bilayers in a Buffer under Osmotic Pressure, J. Phys. Chem. B, 124 (2020) 5588–5599.
[46] B. Brüning, R. Stehle, P. Falus, B. Farago, Influence of charge density on bilayer bending rigidity in lipid vesicles: A combined dynamic light scattering and neutron spin-echo study, Eur. Phys. J. E, 36 (2013) 77.

[47] E. G. Kelley, P. D. Butler, M. Nagao, Collective dynamics in lipid membranes containing transmembrane peptides, Soft Matter, 17 (2021) 5671–5681.
[48] C. Ricci, M. Maccarini, P. Falus, F. Librizzi, M.R. Mangione, O. Moran, M.G. Ortore, R. Schweins, S. Vilasi, R. Carrotta, Amyloid β-Peptide Interaction with Membranes: Can Chaperones Change the Fate?, J. Phys. Chem. B, 123 (2019) 631–638.
[49] J.-H. Lee, S.-M. Choi, C. Doe, A. Faraone, P.A. Pincus, S.R. Kline, Thermal Fluctuation and Elasticity of Lipid Vesicles Interacting with Pore-Forming Peptides, Phys. Rev. Lett., 105 (2010) 038101.
[50] V. Vitkova, P. Méléard, T. Pott, I. Bivas, Alamethicin influence on the membrane bending elasticity, European Biophysics Journal, 35 (2006) 281–286.
[51] G. Pabst, S. Danner, R. Podgornik, J. Katsaras, Entropy-driven softening of fluid lipid bilayers by alamethicin, Langmuir, 23 (2007) 11705–11711.
[52] D. Migoń, M. Jaśkiewicz, D. Neubauer, M. Bauer, E. Sikorska, E. Kamysz, W. Kamysz, Alanine Scanning Studies of the Antimicrobial Peptide Aurein 12, Probiotics & Antimicro. Prot., (2018).
[53] T. Rozek, K.L. Wegener, J.H. Bowie, I.N. Olver, J.A. Carver, J.C. Wallace, M.J. Tyler, The antibiotic and anticancer active aurein peptides from the Australian Bell Frogs Litoria aurea and Litoria raniformis the solution structure of aurein 12, Eur. J. Biochem., 267 (2000) 5330–5341.
[54] E.N. Lorenzón, P.R.S. Sanches, L.G. Nogueira, T.M. Bauab, E.M. Cilli, Dimerization of aurein 12: effects in structure, antimicrobial activity and aggregation of Cândida albicans cells, Amino Acids, 44 (2013) 1521–1528.
[55] V.K. Sharma, S. Qian, Effect of an Antimicrobial Peptide on Lateral Segregation of Lipids: A Structure and Dynamics Study by Neutron Scattering, Langmuir, 35 (2019) 4152–4160.
[56] E.N. Lorenzón, K.A. Riske, G.F. Troiano, G.C.A. Da Hora, T.A. Soares, E.M. Cilli, Effect of dimerization on the mechanism of action of aurein 12, Biochimica et Biophysica Acta (BBA) - Biomembranes, 1858 (2016) 1129–1138.